

## Fission fragment yields in the fission of $^{232}\text{Th}$ by protons of energies 8 to 22 MeV

H. Kudo, H. Muramatsu, and H. Nakahara

*Department of Chemistry, Faculty of Science, Tokyo Metropolitan University, Setagaya, Tokyo, Japan*

K. Miyano

*Department of Physics, Faculty of Science, Niigata University, Niigata, Japan*

I. Kohno

*Institute of Physical and Chemical Research, Wako, Saitama, Japan*

(Received 19 May 1981)

Excitation functions of fission products for 22 fragment masses and neutron-evaporation products,  $(p,n)$ ,  $(p,2n)$ , and  $(p,3n)$ , were measured in detail for the system of  $^{232}\text{Th}+p$  in the proton energy range of 8 to 22 MeV. It was found that the excitation functions of symmetrically divided fission fragments were apparently different from those of asymmetrically divided ones. For the interpretation of the experimental results, a statistical evaporation-and-fission calculation was performed by taking into consideration symmetric and asymmetric fission barriers. The experimental data could be reproduced by this statistical calculation, with fission barrier heights that were in accord with the reported experimental ones for the asymmetric fragments and the theoretically predicted one for the symmetric mass division. The level density parameter at the symmetric saddle had to be about 13% larger than that for the asymmetric saddle in order to reproduce the energy dependence of the cross section ratios of asymmetric to symmetric product yields.

NUCLEAR REACTIONS, FISSION  $^{232}\text{Th}(p,f)$ ,  $E_p=8-22$  MeV, stacked-foil method, excitation functions of fission products and neutron-evaporation products, statistical calculation, symmetric and asymmetric fission barriers.

### I. INTRODUCTION

Many experimental data have been accumulated on various observables associated with nuclear fission since its discovery in 1939.<sup>1</sup> However, no theory for a consistent understanding of those data has been proposed yet, especially for an understanding of the mass yields in fission. Mass distributions in low-energy fission of higher- $Z$  actinide nuclei are typically asymmetric.<sup>2</sup> On the contrary, nuclei of lower  $Z$ , such as Bi and Pb, exhibit symmetric mass distributions.<sup>3-6</sup> For fission of nuclei in the intermediate mass region, such as Ra, Ac, Th, and Pa, triple-humped mass distributions are observed.<sup>7-11</sup>

In 1970, Möller and Nilsson<sup>12</sup> suggested that there might be two kinds of saddle configurations in the fission of  $^{236}\text{U}$ , one with reflection symmetry with respect to an axis perpendicular to the nuclear symmetry axis and the other with reflection asymmetry. The fission barrier for the symmetric saddle

was predicted to be a few MeV higher than the one for the asymmetric saddle. They also hinted that the mode of the final mass division might be in some way governed by which saddle configuration a particular fission motion had experienced. Konecny *et al.*<sup>13</sup> have reported that in the fission of actinium isotopes the symmetric fission barrier heights are higher than the asymmetric ones, and suggested that asymmetric and symmetric fission proceed over different saddle points. These findings are in favor of the view that saddle configurations strongly affect the mode of final mass divisions. On the other hand, another extreme standpoint has been proposed for an explanation of mass distribution which claims that there exist quasistationary states near scission and that the mass distribution can be explained by applying a statistical theory to those states.<sup>14</sup> The existence of such stationary states has not been demonstrated, however, by any theory yet, although Wilkins *et al.*<sup>15</sup> have recently

shown that such a statistical calculation could reproduce mass distributions of fission systems from Po through  $^{258}\text{Fm}$ .

In the present work, we chose the system of proton-induced fission of  $^{232}\text{Th}$  which was known to exhibit a triple-humped mass distribution even with the incident energy of a few tens of MeV.<sup>10</sup> We examined in detail excitation functions of fission products and those of  $(p, xn)$  reactions by a stacked-foil method in the proton energy range of 8 to 22 MeV. Results were examined with the statistical calculation which took into account the existence of two fission barriers.

## II. EXPERIMENTAL

### A. Target preparation

Thorium targets were prepared by electrodeposition onto a  $4\text{ mg/cm}^2$  thick aluminum backing foil from an isopropanol solution at 900 V as described by Aumann and Müllen.<sup>16</sup> Targets were about  $500\text{ }\mu\text{g/cm}^2$  thick, and the amount of  $^{232}\text{Th}$  was determined by neutron activation analysis and by  $\alpha$  spectrometry with a surface barrier detector of known counting efficiency. In the neutron activation analysis, neutron irradiation was performed for 5 min in the thermal column of the reactor of St. Paul's University (thermal neutron flux was about  $5 \times 10^{11}\text{ cm}^{-2}\text{ sec}^{-1}$ ).

The thorium targets thus obtained were wrapped with aluminum cover foils of  $8\text{ mg/cm}^2$  thickness for complete collection of fission products. Five to fifteen of the wrapped targets were then stacked for irradiation. As a proton-energy monitor  $3.12\text{ mg/cm}^2$  thick silver foils and  $10.1\text{ mg/cm}^2$  thick copper foils were inserted into the target stack at appropriate places. Reaction cross sections of silver and copper with protons given by Collé *et al.*<sup>17</sup> were used as references. The proton energy in each target was also calculated from the range-energy relation. The ranges of protons in aluminum, silver, copper, hydrogen, and oxygen were taken from Refs. 18 and 19. As the ranges in thorium were not given therein, those in uranium were used instead. As the thickness of the target was about  $500\text{ }\mu\text{g/cm}^2$ , the error caused by this substitution is negligibly small. The composition of the thorium targets was assumed to be  $\text{Th}(\text{OH})_4 \cdot 1.5\text{ H}_2\text{O}$  (Ref. 20) in this energy calculation.

### B. Proton bombardment

The bombardments were performed at the cyclotron of the Institute of Physical and Chemical

Research and at the cyclotron of the Institute for Nuclear Study of the University of Tokyo. The incident proton energies were varied from 8 to 22 MeV, and the beam current was typically about  $1\text{ }\mu\text{A}$ . The beam current was measured with a Faraday cup equipped with a current integrator. The uncertainties of energy and intensity of the proton beam were at most about 100–200 keV and about 6%, respectively, judging from the cross section of the monitor reactions.

To estimate the effect of neutrons, the proton beam was stopped with an aluminum plate of 10 mm thickness and the target material was placed in the down stream of the beam stopper. No correction was found necessary for the effect of neutrons on the excitation functions of fission products and neutron-evaporation products. The targets were bombarded for periods of 5 to 12 h to ensure adequate intensities of fission product activities.

### C. Chemical separation

For chemical separation of fission products, the irradiated thorium targets with aluminum cover foils were dissolved in hydrochloric acid containing carriers for the elements of interest. The elements were then separated, chemically purified according to the procedures of the ordinary group separation in qualitative analysis.<sup>21,24</sup> The final forms of the separated elements were  $\text{Pd}(\text{C}_4\text{H}_7\text{N}_2\text{O}_2)_2$ , CdS,  $\text{Sb}_2\text{S}_3$ ,  $\text{Ce}(\text{OH})_3$ ,  $\text{Nd}(\text{OH})_3$ , and  $\text{Cs}_2\text{PtCl}_6$ . The chemical yields of the separated elements were determined by neutron activation analysis.

The chemical separation of protoactinium was made according to the procedure proposed by Sill,<sup>25</sup> and electrodeposition onto a stainless steel disk was performed under the condition of a mixed oxalate and ammonium chloride solution.<sup>26</sup> For the determination of chemical and electrodeposition yields the samples were measured before the chemical separation and after the electrodeposition with a Ge(Li) detector for the  $\gamma$  rays from  $^{233}\text{Pa}$  which was produced in the thorium target by neutron irradiation after the proton bombardment.

### D. Activity measurement

For gamma counting the activities produced in the irradiated target sandwiches were measured directly or after chemical separation. The  $\gamma$ -ray spectrometer system was based on a  $40\text{-cm}^3$  Ge(Li) detector equipped with a 2048 pulse height analyzer. The energy resolution of the Ge(Li) detector system was 2.3 keV (FWHM) for the 1.332 MeV  $\gamma$  ray of  $^{60}\text{Co}$ . The gamma decay data of the fission

TABLE I. Fission product and neutron-evaporation product  $\gamma$ -decay data used in excitation function measurements.

Nuclide	Half-life	$E_\gamma$ (keV)	$I_\gamma$ (%)	Reference
$^{87}\text{Kr}$	76.31 min	402.6	$50 \pm 3$	22
$^{88}\text{Kr}$	2.80 h	196	$26.3^a$	23
$^{91}\text{Sr}$	9.48 h	1024	$33 \pm 2$	22
$^{92}\text{Sr}$	2.71 h	1383.94	$90 \pm 10$	22
$^{95}\text{Zr}$	63.98 d	757	$54.6 \pm 0.5$	22
$(^{97}\text{Nb})^b$	72.1 min	658	$98.2 \pm 0.1$	22
$^{99}\text{Mo}$	66.02 h	140.5	$6^a$	22
$(^{99}\text{Tc}^m)^b$	6.02 h	140.5	$89.0 \pm 0.2$	22
$^{103}\text{Ru}$	39.35 d	497.1	$89.35^a$	23
$^{105}\text{Ru}$	4.4 h	469.37	$17.541^a$	23
$(^{112}\text{Ag})^b$	3.12 h	617	$43.3^a$	23
$(^{115}\text{In}^m)^b$	4.49 h	336	$45.9 \pm 0.1$	22
$^{127}\text{Sb}$	3.91 d	783	$14.8 \pm 0.5$	22
$^{128}\text{Sb}^g$	9.1 h	754	$100 \pm 5$	22
$^{129}\text{Sb}$	4.41 h	1030	$13.5 \pm 1.7$	22
$^{132}\text{Te}$	78 h	228	$88 \pm 3$	22
$^{135}\text{I}$	6.61 h	1260.4	$29 \pm 1$	22
$^{136}\text{Cs}$	13 d	818	$99.70 \pm 0.06$	22
$^{141}\text{Ce}$	32.55 d	145	$48.4 \pm 0.4$	22
$^{143}\text{Ce}$	33 h	293	$42^a$	23
$^{147}\text{Nd}$	11.08 d	91	$27.2^a$	23
		531	$13.1^a$	23
$^{149}\text{Pm}$	53.08 h	286	$3.1 \pm 0.2$	22
$^{151}\text{Pm}$	28.4 h	340	$22 \pm 1$	22
$^{232}\text{Pa}$	1.31 d	969.2	$44.6^a$	22
$^{230}\text{Pa}$	17.7 d	952	$28.3^a$	22

<sup>a</sup>Uncertainty of  $\pm 10\%$  assumed.

<sup>b</sup>In equilibrium with parent nuclide.

products and those of neutron-evaporation products selected for use in this work are tabulated in Table I. The measured  $\gamma$ -ray activities were corrected for counting efficiency, photon abundance, genetic relationships, degree of saturation during bombardment, and the target amount to give excitation functions. The uncertainties in the determination of cross sections were estimated to be about 8% based on those associated with absolute photon abundance (1–10%), absolute detector efficiency ( $\sim 5\%$ ), and chemical separation ( $\sim 3\%$ ).

Protoactinium-231, the  $(p, 2n)$  reaction product, is an  $\alpha$ -particle emitter, and has a long half-life of  $3.28 \times 10^4$  y. The  $\alpha$  particles of 5.05 MeV (10%), 5.02 MeV (23%), 5.01 MeV (24%), 4.98 MeV (2.3%), 4.94 MeV (22%), and 4.93 MeV (2.8%) of  $^{231}\text{Pa}$  were measured with a Si(Au) surface barrier detector for 7 to 10 d for each sample.

In order to obtain the  $^{232}\text{Th}$  target amount, a neutron irradiation was performed before the deter-

mination of  $^{231}\text{Pa}$ . Therefore, the effect of  $^{232}\text{Th}(n, 2n)^{231}\text{Th}\beta^-/25.5 \text{ h} \rightarrow ^{231}\text{Pa}$  had to be estimated for the precise determination of the  $^{232}\text{Th}(p, 2n)^{231}\text{Pa}$  reaction cross section. For this purpose, thorium which had not been bombarded with protons was irradiated by neutrons at the same time with the thorium targets, and the same procedure for protoactinium chemical separation followed by electrodeposition was performed. It was found unnecessary to correct for the effect of neutron irradiation on the determination of  $^{231}\text{Pa}$  since no  $\alpha$  particles of  $^{231}\text{Pa}$  were detected from the neutron-irradiated thorium sample of nonproton bombardment.

### III. RESULTS AND DISCUSSION

The excitation functions of 22 fission products in the proton induced fission of  $^{232}\text{Th}$  were obtained in

TABLE II. Formation cross sections (mb) of fission products in proton-induced fission of  $^{232}\text{Th}$ . The numbers in parentheses are the number of experiments.

Proton energy (MeV)	$^{87}\text{Kr}$	$^{88}\text{Kr}$	$^{91}\text{Sr}$	$^{92}\text{Sr}$	$^{95}\text{Zr}$	$^{97}\text{Zr}(\text{Nb})$	$^{99}\text{Mo}(\text{Tc})$	$^{103}\text{Ru}$	$^{105}\text{Ru}$	$^{112}\text{Pd}(\text{Ag})$	$^{115}\text{Cd}(\text{In})$
21.9	32.6 ± 4.7(2)	36.0 ± 4.8(2)	50.5 ± 5.3(2)	44.0 ± 6.2(2)		39.0 ± 3.3(2)	33.8 ± 2.9(2)		28.8 ± 4.4(2)	32.6 ± 4.3(2)	33.4 ± 2.8(1)
21.3	49.4 ± 6.4(1)	36.0 ± 4.8(1)	50.4 ± 5.4(1)	46.6 ± 6.6(1)		37.5 ± 3.2(1)	33.1 ± 2.8(1)		23.8 ± 4.6(1)	31.6 ± 4.1(1)	31.9 ± 2.7(1)
21.0	36.3 ± 5.0(1)	34.6 ± 5.2(2)	50.0 ± 5.4(2)	41.6 ± 6.2(2)	48.4 ± 4.2(1)	37.7 ± 3.2(2)	32.9 ± 4.1(2)	30.5 ± 4.0(1)	24.7 ± 3.5(1)	31.9 ± 4.3(2)	37.3 ± 3.2(1)
20.6	44.9 ± 5.5(1)	43.3 ± 5.7(1)	59.0 ± 6.2(1)	52.2 ± 7.3(1)		30.7 ± 2.6(1)	38.5 ± 3.3(1)		23.6 ± 4.4(1)	33.8 ± 4.4(1)	33.2 ± 2.8(1)
20.2	42.7 ± 5.1(1)	36.6 ± 5.3(2)	53.2 ± 5.6(2)	42.5 ± 6.2(2)	36.6 ± 3.1(1)	36.2 ± 3.1(2)	30.7 ± 2.7(2)	25.9 ± 3.4(1)	20.8 ± 3.3(2)	26.5 ± 3.5(2)	27.8 ± 2.5(1)
20.0	45.6 ± 5.6(1)	42.9 ± 5.7(1)	52.9 ± 5.6(1)	51.9 ± 7.3(1)		40.9 ± 3.5(1)	35.6 ± 3.1(1)		23.6 ± 4.3(1)	29.4 ± 3.8(1)	27.2 ± 2.3(1)
19.5	44.2 ± 5.3(1)	46.6 ± 8.9(2)	54.0 ± 5.7(2)	38.6 ± 5.6(2)	43.3 ± 3.7(1)	38.5 ± 3.3(2)	33.1 ± 2.8(2)	24.5 ± 3.2(1)	17.1 ± 2.7(1)	26.8 ± 3.5(2)	23.7 ± 2.1(2)
19.3	44.5 ± 5.1(1)	44.6 ± 5.8(1)	58.2 ± 6.1(1)	50.0 ± 7.0(1)		39.9 ± 3.4(1)	32.7 ± 2.9(1)		21.9 ± 3.1(1)	29.4 ± 3.9(1)	
19.0	50.2 ± 5.7(1)	39.9 ± 5.7(2)	53.0 ± 5.6(2)	48.9 ± 7.0(2)	46.3 ± 4.0(1)	36.8 ± 3.1(2)	32.4 ± 2.8(2)	25.0 ± 3.3(1)	17.6 ± 2.8(1)	24.9 ± 3.3(2)	24.8 ± 2.2(2)
18.4	43.0 ± 4.8(2)	41.6 ± 5.7(3)	55.2 ± 5.8(3)	50.5 ± 7.1(3)	47.5 ± 4.0(2)	36.7 ± 3.1(3)	32.9 ± 2.8(3)	22.1 ± 2.9(1)	21.3 ± 3.1(2)	22.8 ± 3.0(3)	23.4 ± 2.4(2)
17.7	52.8 ± 5.7(2)	42.7 ± 5.8(3)	57.3 ± 6.0(3)	51.4 ± 7.3(3)	55.9 ± 4.8(2)	36.0 ± 3.1(3)	31.2 ± 2.7(3)	21.8 ± 2.8(1)	17.6 ± 2.6(2)	22.4 ± 3.0(3)	19.5 ± 1.7(2)
17.0	50.1 ± 9.0(2)	42.1 ± 5.6(3)	53.7 ± 5.6(3)	47.3 ± 6.7(3)	44.0 ± 3.8(2)	33.5 ± 2.9(3)	29.8 ± 2.6(3)	18.5 ± 2.5(1)	14.5 ± 2.1(2)	20.0 ± 2.7(3)	17.0 ± 1.5(2)
16.6	42.0 ± 4.6(1)	34.5 ± 4.7(2)	48.1 ± 5.1(2)	40.2 ± 5.7(2)	41.9 ± 3.6(1)	30.2 ± 2.6(2)	27.4 ± 2.4(2)	13.7 ± 1.8(1)	12.6 ± 1.9(1)	15.2 ± 2.0(2)	14.4 ± 1.3(2)
16.0	32.7 ± 3.5(2)	25.6 ± 5.1(3)	36.4 ± 3.8(3)	29.1 ± 5.6(3)	41.8 ± 3.6(1)	25.1 ± 2.9(3)	23.0 ± 2.0(3)	14.2 ± 1.9(1)	10.2 ± 3.2(2)	11.8 ± 1.7(3)	11.9 ± 1.2(2)
15.7	27.4 ± 2.9(1)	27.1 ± 3.6(2)	30.9 ± 3.2(2)	29.1 ± 4.1(2)		19.4 ± 1.6(2)	17.9 ± 1.6(2)		8.6 ± 1.3(2)	8.8 ± 1.2(2)	9.3 ± 0.8(2)
15.4	25.8 ± 2.7(1)	20.3 ± 4.4(3)	26.9 ± 3.0(3)	23.1 ± 5.0(3)	28.7 ± 2.8(1)	19.7 ± 2.4(3)	19.4 ± 3.3(3)	10.1 ± 1.4(1)	9.4 ± 2.9(2)	8.4 ± 1.2(3)	7.6 ± 0.6(1)
14.8	15.4 ± 2.0(3)	15.4 ± 2.0(4)	19.1 ± 2.0(4)	18.7 ± 2.6(4)	16.5 ± 1.5(2)	14.7 ± 1.3(4)	14.3 ± 4.7(4)	5.9 ± 0.8(1)	6.2 ± 1.7(4)	6.0 ± 0.9(4)	5.9 ± 0.5(1)
14.3	11.2 ± 1.3(3)	11.1 ± 1.5(4)	15.0 ± 1.6(4)	14.4 ± 2.0(4)	12.1 ± 1.5(2)	12.2 ± 1.0(4)	10.6 ± 2.3(4)	3.8 ± 0.5(1)	5.4 ± 1.2(3)	5.4 ± 0.8(4)	4.8 ± 0.4(1)
13.9	9.4 ± 1.1(2)	8.1 ± 1.1(3)	11.3 ± 1.2(4)	11.2 ± 1.6(4)	10.2 ± 0.9(2)	9.5 ± 0.8(4)	8.7 ± 1.7(4)	4.2 ± 0.6(1)	3.8 ± 0.9(3)	4.1 ± 0.6(4)	3.9 ± 0.3(2)
13.5	6.8 ± 0.8(1)	8.0 ± 1.7(2)	10.7 ± 1.3(3)	10.1 ± 1.5(3)		8.8 ± 1.0(3)	10.4 ± 2.9(3)		4.6 ± 1.2(2)	2.9 ± 0.5(3)	3.3 ± 0.3(2)
13.3	6.8 ± 0.8(1)	8.2 ± 1.1(2)	10.5 ± 1.1(2)	10.7 ± 1.5(2)	9.4 ± 0.9(2)	9.3 ± 0.9(2)	10.2 ± 4.3(2)	3.8 ± 0.5(1)	3.1 ± 0.4(1)	3.2 ± 0.5(2)	
13.0	7.9 ± 1.7(2)	6.8 ± 1.3(2)	8.5 ± 0.9(3)	8.2 ± 1.2(3)		7.1 ± 0.8(3)	8.4 ± 3.4(3)		3.7 ± 0.6(2)	2.5 ± 0.7(3)	2.3 ± 0.2(2)
12.7	6.0 ± 0.6(2)	5.8 ± 0.8(3)	7.2 ± 0.8(3)	7.3 ± 1.0(3)	6.6 ± 0.6(2)	6.7 ± 0.6(3)	8.6 ± 3.0(3)	2.0 ± 0.3(1)	2.7 ± 0.6(2)	2.1 ± 0.5(2)	
12.4	5.3 ± 0.9(2)	4.5 ± 0.6(2)	6.5 ± 0.7(3)	6.1 ± 0.9(3)	5.2 ± 0.4(1)	5.1 ± 0.4(3)	5.0 ± 0.7(3)		1.59 ± 0.23(2)	1.57 ± 0.21(3)	1.68 ± 0.15(2)
11.9	4.7 ± 0.6(2)	4.2 ± 0.6(3)	5.5 ± 0.6(4)	5.3 ± 0.8(4)	5.0 ± 0.5(2)	4.4 ± 0.4(4)	5.1 ± 1.2(4)	1.38 ± 0.21(1)	0.97 ± 0.28(2)	1.07 ± 0.18(4)	1.17 ± 0.13(2)
11.3	3.0 ± 0.4(2)	2.9 ± 0.4(3)	3.8 ± 0.4(4)	3.4 ± 0.6(4)	3.5 ± 0.3(2)	2.9 ± 0.3(4)	4.3 ± 1.3(4)	0.91 ± 0.15(1)	0.56 ± 0.10(1)	0.66 ± 0.10(4)	0.66 ± 0.07(2)
10.6	2.3 ± 0.3(2)	2.2 ± 0.3(2)	2.8 ± 0.3(3)	2.6 ± 0.4(3)	2.2 ± 0.2(1)	2.0 ± 0.2(3)	3.1 ± 0.5(3)		0.37 ± 0.06(3)	0.37 ± 0.06(3)	0.43 ± 0.04(2)
9.9	1.04 ± 0.12(1)	1.09 ± 0.14(1)	1.44 ± 0.17(2)	1.31 ± 0.21(2)	1.17 ± 0.10(1)	1.09 ± 0.10(2)	2.1 ± 0.5(2)		0.145 ± 0.02(1)	0.23 ± 0.02(1)	0.23 ± 0.02(1)
9.3	0.42 ± 0.06(1)	0.49 ± 0.07(1)	0.84 ± 0.14(2)	0.65 ± 0.11(2)	0.49 ± 0.05(1)	0.57 ± 0.07(2)	1.34 ± 0.12(2)		0.088 ± 0.013(1)	0.101 ± 0.011(1)	0.101 ± 0.011(1)
8.6	0.12 ± 0.02(1)	0.14 ± 0.03(1)	0.25 ± 0.03(2)	0.23 ± 0.08(2)	0.20 ± 0.03(1)	0.20 ± 0.07(2)	0.78 ± 0.07(2)		0.033 ± 0.005(1)	0.037 ± 0.005(1)	0.037 ± 0.005(1)
7.9				0.21 ± 0.09(1)		0.041 ± 0.012(1)	0.39 ± 0.04(1)		0.010 ± 0.002(1)	0.008 ± 0.002(1)	

TABLE II. (Continued.)

Proton energy (MeV)	$^{127}\text{Sb}$	$^{128}\text{Sb}$	$^{129}\text{Sb}$	$^{132}\text{Te}$	$^{135}\text{I}$	$^{136}\text{Cs}$	$^{141}\text{Ce}$	$^{143}\text{Ce}$	$^{147}\text{Nd}$	$^{149}\text{Pm}$	$^{151}\text{Pm}$
21.9	16.8 ± 1.5(1)	4.86 ± 0.47(1)	5.21 ± 0.97(1)	29.2 ± 2.8(2)	29.3 ± 2.8(2)	6.17 ± 0.53(1)	42.2 ± 3.6(1)	39.8 ± 5.2(2)	14.2 ± 1.9(1)	9.3 ± 1.1(1)	2.79 ± 0.27(1)
21.3				30.2 ± 2.8(1)	28.5 ± 2.8(1)	5.58 ± 0.48(1)		36.3 ± 4.9(1)			
21.0	14.6 ± 1.3(1)	4.42 ± 0.43(1)	5.38 ± 0.94(1)	30.7 ± 2.9(2)	30.6 ± 3.1(2)		47.9 ± 4.0(1)	42.4 ± 5.6(2)	15.3 ± 2.0(1)	8.6 ± 1.0(1)	2.66 ± 0.26(1)
20.6				19.4 ± 1.9(1)	35.2 ± 3.4(1)	6.35 ± 0.54(1)		45.1 ± 6.0(1)			
20.2	14.4 ± 1.3(1)	4.20 ± 0.41(1)	7.9 ± 1.2(1)	30.5 ± 2.8(2)	33.9 ± 3.3(2)		49.3 ± 4.2(2)	42.3 ± 5.5(2)	16.7 ± 2.2(1)	9.3 ± 1.1(1)	2.80 ± 0.27(1)
20.0				32.5 ± 3.0(1)	37.1 ± 3.6(1)	5.71 ± 0.49(1)		47.0 ± 6.2(1)			
19.5				31.9 ± 2.9(2)	34.2 ± 3.4(2)	4.82 ± 0.41(1)		45.7 ± 6.1(2)			
19.3	15.3 ± 1.4(1)	4.25 ± 0.41(1)	6.5 ± 1.0(1)	30.7 ± 2.9(1)	39.2 ± 3.7(1)		51.1 ± 4.3(1)	52.0 ± 6.8(1)	21.5 ± 2.8(1)	12.2 ± 1.4(1)	3.11 ± 0.30(1)
19.0				32.6 ± 3.0(2)	37.0 ± 3.6(2)	4.45 ± 0.38(1)	56.8 ± 4.8(1)	45.2 ± 6.8(2)			
18.4	13.5 ± 1.2(1)	3.39 ± 0.32(1)	6.6 ± 1.0(1)	32.5 ± 3.0(3)	38.1 ± 3.6(3)	4.11 ± 0.35(1)	58.7 ± 5.0(2)	51.3 ± 6.7(3)	18.5 ± 2.4(1)	10.1 ± 1.1(1)	2.87 ± 0.28(1)
17.7	11.6 ± 1.1(1)	3.34 ± 0.33(1)	6.6 ± 1.1(1)	28.4 ± 3.3(3)	39.7 ± 3.7(3)	3.51 ± 0.30(1)	59.9 ± 5.1(2)	53.6 ± 7.0(3)	17.6 ± 2.3(1)	10.7 ± 1.2(1)	2.66 ± 0.26(1)
17.0	10.3 ± 0.9(1)	2.87 ± 0.28(1)	5.54 ± 0.88(1)	29.5 ± 4.1(3)	37.7 ± 3.6(3)	3.31 ± 0.28(1)	56.1 ± 6.4(2)	52.2 ± 7.7(3)	15.7 ± 2.0(1)	8.9 ± 1.0(1)	2.44 ± 0.24(1)
16.6				27.6 ± 4.1(2)	35.6 ± 3.4(2)	3.01 ± 0.26(1)	54.2 ± 4.6(1)	47.7 ± 6.7(2)			
16.0	7.40 ± 0.70(1)	2.03 ± 0.20(1)	5.35 ± 0.91(1)	22.7 ± 3.0(3)	25.8 ± 2.5(3)	2.07 ± 0.18(1)	46.6 ± 6.5(2)	38.7 ± 7.5(3)	13.6 ± 1.8(1)	7.67 ± 0.87(1)	2.00 ± 0.20(1)
15.7				17.2 ± 1.6(2)	23.3 ± 2.2(2)	1.77 ± 0.15(2)		30.6 ± 4.0(2)			
15.4	6.99 ± 0.65(1)	2.14 ± 0.21(1)	4.90 ± 0.76(1)	18.3 ± 3.2(3)	20.8 ± 2.7(2)	1.50 ± 0.13(1)	37.3 ± 5.2(2)	29.9 ± 4.0(3)	10.4 ± 1.4(1)	7.09 ± 0.83(1)	1.74 ± 0.17(1)
14.8	4.99 ± 0.46(2)	1.46 ± 0.14(2)	3.41 ± 0.53(2)	12.3 ± 1.2(4)	15.3 ± 1.5(4)	1.12 ± 0.10(1)	21.3 ± 2.4(3)	17.0 ± 2.3(4)	6.42 ± 0.83(2)	4.15 ± 0.50(2)	1.28 ± 0.13(2)
14.3	3.81 ± 0.37(2)	1.07 ± 0.11(2)	2.45 ± 0.40(2)	10.1 ± 0.9(4)	12.5 ± 1.2(4)	0.81 ± 0.07(2)	15.3 ± 1.3(3)	12.7 ± 1.7(3)	5.13 ± 0.67(2)	2.82 ± 0.36(2)	1.11 ± 0.11(2)
13.9	3.61 ± 0.34(2)	1.03 ± 0.10(2)	2.28 ± 0.36(1)	8.2 ± 1.0(4)	9.73 ± 0.91(4)	0.610 ± 0.055(2)	10.9 ± 1.7(3)	9.6 ± 1.5(4)	3.97 ± 0.54(2)	2.29 ± 0.29(2)	0.90 ± 0.09(2)
13.5	2.87 ± 0.28(2)	0.84 ± 0.08(2)	1.77 ± 0.29(1)	7.8 ± 1.2(3)	8.3 ± 1.2(3)	0.495 ± 0.045(2)	10.9 ± 1.7(2)	9.3 ± 1.4(3)	3.84 ± 0.61(2)	2.04 ± 0.63(2)	0.81 ± 0.08(2)
13.3	2.69 ± 0.26(1)	0.80 ± 0.08(1)	2.06 ± 0.33(1)	7.75 ± 0.75(2)	9.35 ± 0.91(2)		10.6 ± 1.1(2)	8.9 ± 1.2(3)	3.24 ± 0.42(1)	1.84 ± 0.22(1)	0.83 ± 0.08(1)
13.0	1.98 ± 0.19(2)	0.56 ± 0.06(2)	1.55 ± 0.25(1)	5.94 ± 0.68(3)	7.2 ± 1.2(3)	0.374 ± 0.079(2)	8.7 ± 1.7(2)	7.6 ± 1.4(3)	3.13 ± 0.56(2)	1.74 ± 0.43(2)	0.71 ± 0.07(2)
12.7	1.42 ± 0.15(2)	0.44 ± 0.11(2)	1.33 ± 0.21(2)	5.44 ± 0.73(3)	6.41 ± 0.64(3)		7.47 ± 0.63(2)	6.31 ± 0.90(3)	2.61 ± 0.34(2)	1.60 ± 0.21(2)	0.54 ± 0.06(2)
12.4	1.44 ± 0.16(2)	0.38 ± 0.04(2)	0.91 ± 0.16(1)	4.55 ± 0.42(3)	5.61 ± 0.54(3)	0.256 ± 0.024(2)	5.93 ± 0.50(2)	5.44 ± 0.71(3)	2.03 ± 0.26(2)	1.03 ± 0.16(2)	0.45 ± 0.05(2)
11.9	1.10 ± 0.11(2)	0.30 ± 0.03(2)	1.07 ± 0.17(1)	3.87 ± 0.37(4)	4.71 ± 0.46(4)	0.191 ± 0.018(2)	5.53 ± 0.56(3)	4.42 ± 0.60(4)	1.75 ± 0.23(2)	0.93 ± 0.13(2)	0.41 ± 0.07(2)
11.3	0.68 ± 0.08(2)	0.19 ± 0.02(2)	0.63 ± 0.10(1)	2.40 ± 0.24(4)	3.14 ± 0.40(4)	0.114 ± 0.011(2)	3.55 ± 0.43(3)	3.47 ± 0.47(4)	1.28 ± 0.17(2)	0.70 ± 0.14(2)	0.291 ± 0.034(2)
10.6	0.40 ± 0.05(2)	0.11 ± 0.01(2)	0.43 ± 0.07(1)	1.66 ± 0.17(3)	2.34 ± 0.24(3)	0.078 ± 0.014(2)	2.61 ± 0.22(2)	2.44 ± 0.32(3)	0.85 ± 0.11(2)	0.53 ± 0.08(2)	0.180 ± 0.021(2)
9.9	0.215 ± 0.033(2)	0.052 ± 0.006(2)	0.20 ± 0.04(1)	0.87 ± 0.10(2)	1.09 ± 0.13(2)	0.044 ± 0.007(1)	1.93 ± 0.64(2)	1.22 ± 0.16(2)	0.50 ± 0.07(2)	0.21 ± 0.04(2)	0.112 ± 0.021(2)
9.3	0.103 ± 0.038(2)	0.029 ± 0.007(2)	0.052 ± 0.011(1)	0.48 ± 0.06(2)	0.81 ± 0.26(2)	0.019 ± 0.004(1)	0.76 ± 0.16(2)	0.68 ± 0.17(2)	0.24 ± 0.03(2)	0.076 ± 0.040(2)	0.066 ± 0.012(2)
8.6	0.044 ± 0.010(2)	0.008 ± 0.001(2)	0.035 ± 0.009(1)	0.18 ± 0.03(2)	0.28 ± 0.14(2)	0.009 ± 0.003(1)	0.26 ± 0.05(2)	0.23 ± 0.05(2)	0.139 ± 0.022(2)		0.039 ± 0.008(1)
7.9	0.013 ± 0.006(1)	0.004 ± 0.001(1)		0.081 ± 0.021(1)	0.116 ± 0.036(1)	0.007 ± 0.002(1)	0.095 ± 0.008(1)	0.081 ± 0.011(1)	0.035 ± 0.007(1)		

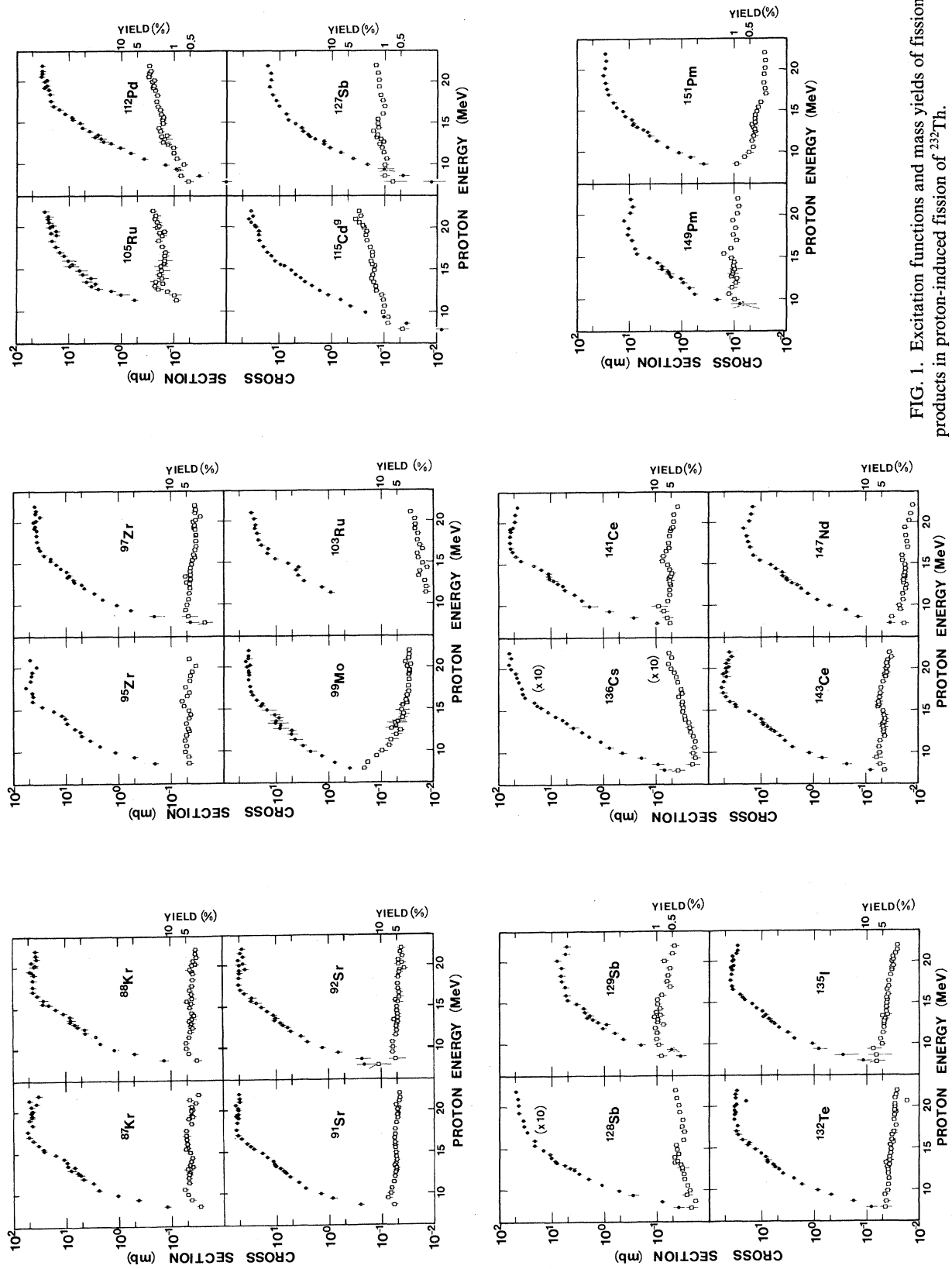


FIG. 1. Excitation functions and mass yields of fission products in proton-induced fission of  $^{232}\text{Th}$ .

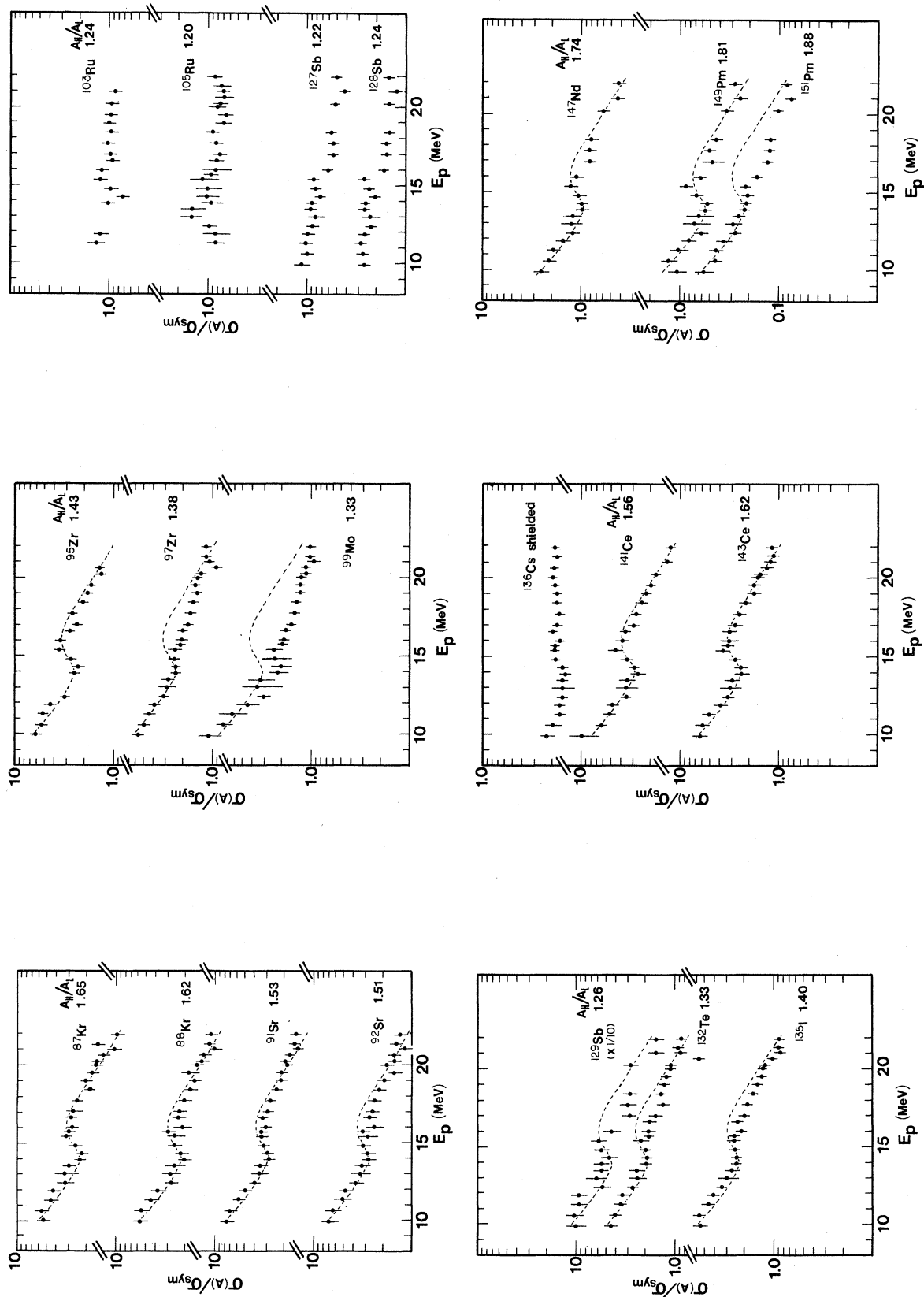


FIG. 2. Cross section ratios  $\sigma(A)/\sigma_{\text{sym}}$  as a function of the incident proton energy. The averages of the yield of  $^{112}\text{Pd}$  and  $^{115}\text{Cd}$  are used for  $\sigma_{\text{sym}}$ . The dashed lines are the results of theoretical calculation for  $\sigma_{\text{asym}}/\sigma_{\text{sym}}$  in arbitrary magnitude.

the proton energy range of 8 to 22 MeV. The results are summarized in Table II and shown in Fig. 1. They are not corrected for the effect of neutron evaporation from primary fragments. The vertical line attached to each data point indicates the range of one standard deviation associated with the activity counting statistics, the uncertainties described before, and the difference between each run in the case of two or more runs. It is found from the figures that the proton energy dependences of the excitation functions of asymmetrically divided fission products are similar to each other except for  $^{136}\text{Cs}$  which is one of the shielded nuclides. The dependence is also similar for symmetrically divided fission products among themselves, but different from those for the asymmetrically divided products. The cross sections of the symmetrically divided products increase monotonically with proton energy. On the other hand, the excitation functions of the asymmetrically divided products seem to level off or even decrease above 17 MeV with some structure at  $\sim 14$  MeV. The different energy dependence can be more clearly depicted if the cross section ratios of asymmetric to symmetric products are plotted as given in Fig. 2. As the representative symmetric product cross sections, the averages of  $^{112}\text{Pd}$  and  $^{115}\text{Cd}$  were taken. The mass ratios ( $A_H/A_L$ ) of the complementary fragment pairs are also indicated in the figure where subscripts  $H$  and  $L$  denote the heavy and light product, respectively. For evaluation of mass ratios, one neutron was assumed to be evaporated from each fragment after fission of  $^{233}\text{Pa}$ . The cross section data were, however, not corrected for any neutron emission which was expected either before and/or after fission. The cross section ratios for the products with  $A_H/A_L > 1.25$  are found strongly decreasing with about the same overall slope (within the experimental error of one standard deviation) as the incident proton energy is increased. ( $^{99}\text{Mo}$  and  $^{151}\text{Pm}$  seem to decrease somewhat more steeply.) For those asymmetric products, some structure, namely, local minimum and maximum, is observed at energies around 14 and 16 MeV, respectively, although it is not distinctive for  $^{92}\text{Sr}$ ,  $^{97}\text{Zr}$ ,  $^{99}\text{Mo}$ ,  $^{129}\text{Sb}$ ,  $^{132}\text{Te}$ , and  $^{151}\text{Pm}$ . The energy dependence of the ratio for  $^{136}\text{Cs}$  is quite different from those for asymmetric products and it shows almost zero slope. For products with  $A_H/A_L < 1.25$ , the ratios are less energy dependent and they change at most by a factor of 2 within the energy range investigated. It is also to be mentioned that  $^{129}\text{Sb}$ ,  $^{132}\text{Te}$ , and  $^{135}\text{I}$  are expected to lie close to the most probable charge  $Z_p$  in their

respective isobaric charge distribution. Therefore, these yields might be sensitive to the shift of  $Z_p$  as the incident energy was varied.

In the past several investigations measured peak-to-trough ratios as a function of incident particle energy for various fissioning systems.<sup>27-32</sup> They observed some structure similar to the ones shown in Fig. 2. The incident particle energies where local rises were observed in the ratio curves were shown to coincide with the energies where new channels for the next-higher-order multiple-chance fission were opened.<sup>29</sup> It has also been pointed out by many investigators that symmetric fission becomes more favored as the energy applied to the fissioning nucleus is increased.<sup>33</sup> The local rise in the ratio

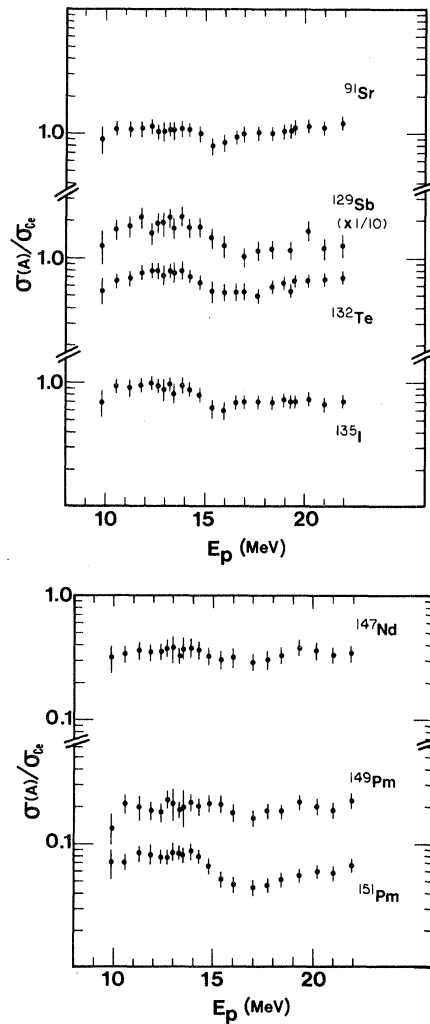


FIG. 3. Cross section ratios among asymmetric fission products as a function of the incident proton energy. The averages of the yields of  $^{141}\text{Ce}$  and  $^{143}\text{Ce}$  are used as the denominators.

curve is, therefore, generally interpreted as due to the onset of the next-higher-order multiple-chance fission in which asymmetric fission becomes more probable than symmetric fission because of cooling of the fissioning nucleus caused by the preceding neutron emission. The peak energy of about 16 MeV observed in this work is in agreement with the  $16.4 \pm 0.5$  MeV reported by Bowles *et al.* for the ( $^{232}\text{Th} + p$ ) reaction system,<sup>29</sup> and it corresponds to the energy where the contribution of the ( $p, 2nf$ ) becomes appreciable.

In Fig. 3 are plotted cross section ratios among asymmetric fission products of heavier masses. As the denominator, averages of the  $^{141}\text{Ce}$  and  $^{143}\text{Ce}$  cross sections were chosen. The ratio for  $^{91}\text{Sr}$  is also given in the figure in order to show the behavior of the lighter asymmetric fission products. The energy dependence of the ratios is found small for all the cases and for some, there seems to be a decrease beginning around 14–15 MeV. Within the statistical error of one standard deviation, the energy variation of the ratio is, however, not very significant and it is at most by a factor of 2 in the energy range investigated. It is interesting to note that the ratios for  $^{149}\text{Pm}$  and  $^{151}\text{Pm}$  which are the products of extremely asymmetric mass divisions ( $A_H/A_L = 1.81$  and 1.88) show energy dependence similar to those for high-yield asymmetric products. It is also to be pointed out that the energy dependence of the ratios among asymmetric fission products are not significantly different from that of the ratios among symmetric products. (See  $^{103}\text{Ru}$ ,  $^{105}\text{Ru}$ ,  $^{127}\text{Sb}$ , and  $^{128}\text{Sb}$  in Fig. 2.)

The mass yield curve can be constructed from the excitation functions of individual fission products for a specific incident energy of protons. It was assumed as a first approximation that the charge dispersion of fission products shows a Gaussian distribution with the most probable charge  $Z_p$  expected from the uncharged charge distribution model and the width parameter taken to 0.95,<sup>34</sup> although the experimental  $Z_p$  is reported to vary with fragment mass, fissioning nucleus, and excitation energy.<sup>35</sup> The results are depicted in Fig. 4. It is seen that the symmetric mass divisions become comparable in cross section to the asymmetric mass divisions as the proton energy increases. The total fission cross section was evaluated by summing the cross section of each mass and is shown in Fig. 5, together with the excitation functions of neutron-evaporation products. The comparison with the reported data<sup>27,28,36–38</sup> is shown in Fig. 6. The present data are smaller than those of Refs. 36 and

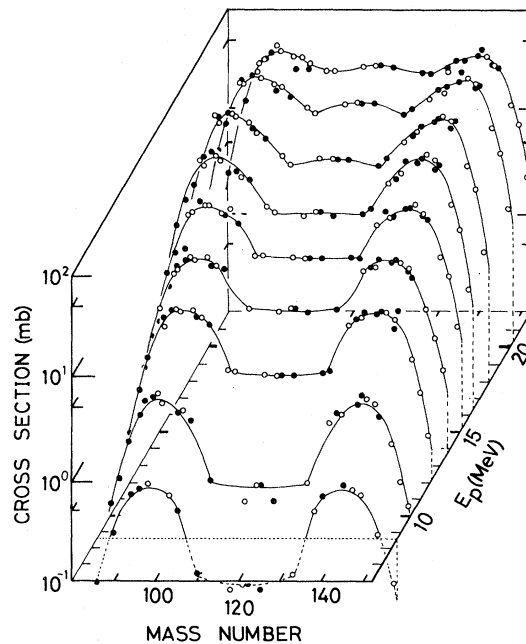


FIG. 4. Mass yield curves measured in proton-induced fission of  $^{232}\text{Th}$ .

38 at proton energies below 12 MeV and larger than those of Ref. 38 at energies above 16 MeV.

Next, the energy dependence of the fission yield,

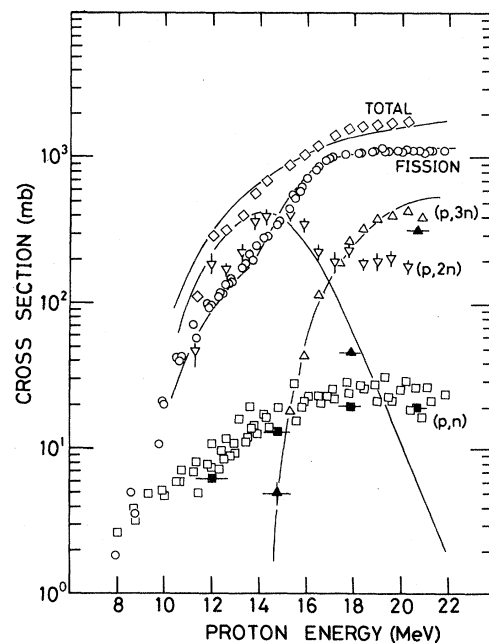


FIG. 5. Excitation functions of fission and neutron-evaporation reaction in  $^{232}\text{Th} + p$  system. Closed symbols are those obtained by Tewe (1955) for ( $p, n$ ) (■) and ( $p, 3n$ ) (▲). Solid lines are the results of the statistical calculation.

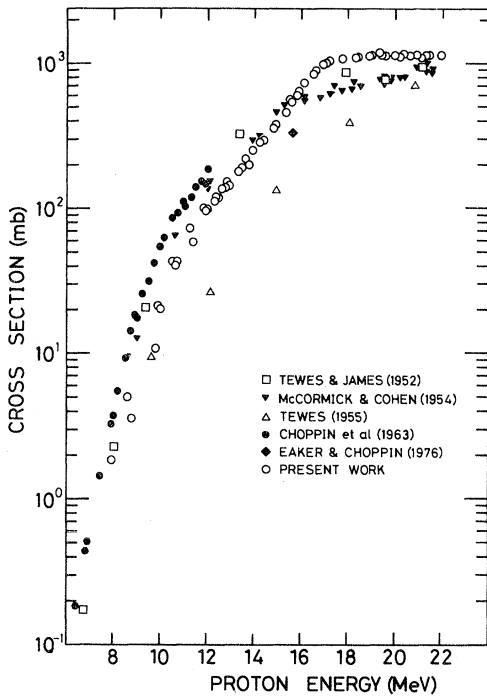


FIG. 6. Measured fission cross section in proton-induced fission of  $^{232}\text{Th}$ .

defined as the ratio of the formation cross section to the total fission cross section, was examined for completeness of the data analysis. The results are shown in Fig. 1 as open squares. As described above, it was found in the present work that the incident energy dependence of symmetric fission product yields was much steeper than that for asymmetric product yields, and that asymmetric products and symmetric products showed similar energy dependence among themselves within the energy range investigated. This observation suggests that symmetric mass divisions require some extra energy which is much larger than the energy variation expected for different degrees of mass asymmetries within each division mode. If there is only one kind of saddle point, and if fission probability is determined at the saddle as originally proposed by Bohr and Wheeler,<sup>39</sup> the extra threshold energy necessary for symmetric mass divisions has to be claimed somewhere between the saddle and the scission point. Recently, Wilkins *et al.*<sup>15</sup> calculated potential energies of scission configurations by the microscopic approach and found that for the  $^{227}\text{Ra}$  system, the potential energy for symmetric mass divisions could be larger than the saddle-point barrier energy. As they pointed out, this kind of threshold energy can appear only for those fission

systems where the saddle configuration is close to the scission configuration. (The  $Z^2/A$  for  $^{227}\text{Ra}$  is 34.11.) For the systems of larger  $Z^2/A$  like the one used in this work (for  $^{233}\text{Pa}$ ,  $Z^2/A = 35.54$ ), the minimum potential energy at the scission point for all mass splits lies well below the saddle point energy, and no such threshold is expected to occur. For those systems, if the scission-point model is assumed, the excitation function of each fission product ( $Z_1, A_1$ ) is expressed by the product of two factors: the probability of formation of a compound nucleus with subsequent decay by fission and the probability of the fission process resulting in the specific charge  $Z_1$  and mass  $A_1$  division which is determined by the potential energy and the collective temperature near scission. In order to compare the theory with the present results, the former probability has to be calculated with inclusion of the competition between neutron emission and fission, and the latter probability with proper consideration of the variation in effective intrinsic temperature as the incident particle energy is varied.

In the following, another model is used to explain the present data: namely, the extra threshold energy is assumed to originate from the difference in barrier height between two kinds of saddle points, one for asymmetric fission and the other for symmetric fission in order to explain the experimental results of the asymmetric-to-symmetric ratios shown in Fig. 2 and, also, to explain the excitation functions of neutron-evaporation products and total fission. Statistical calculations were performed with the ALICE code<sup>40</sup> which was modified to include symmetric fission barriers and asymmetric fission barriers as parameters. This modification is essentially the division of the fission width,  $\Gamma_f$ , into the asymmetric fission width,  $\Gamma_{f,a}$ , and the symmetric fission width,  $\Gamma_{f,s}$ , implying the existence of competition among asymmetric fission, symmetric fission, and neutron emission. The effect of barrier penetration was also included<sup>41</sup> as a modification.

The following parameters were used in the calculation:  $a_n$ , level density parameter at ground state deformation;  $a_{f,a}$ , level density parameter at asymmetric saddle point deformation;  $a_{f,s}$ , level density parameter at symmetric saddle point deformation;  $\hbar\omega_a$ , barrier curvature energy for asymmetric fission;  $\hbar\omega_s$ , barrier curvature energy for symmetric fission;  $E_{f,a1}$ ,  $E_{f,a2}$ ,  $E_{f,a3}, \dots$ , asymmetric fission barrier heights; and  $E_{f,s1}$ ,  $E_{f,s2}$ ,  $E_{f,s3}, \dots$ , symmetric fission barrier heights.

The experimental excitation functions could be well reproduced with the statistical calculation as

TABLE III. Used parameters in the statistical calculation.

Mode of fission	Multiple chance fission	$E_f$ (MeV)	$a_n$ (MeV $^{-1}$ )	$a_f/a_n$	$\hbar\omega$ (MeV)
Asymmetric fission	( $p, f$ )	5.9			
	( $p, nf$ )	6.2	$A/8$	1.02	1.0
	( $p, 2nf$ )	6.0			
Symmetric fission	( $p, f$ )	8.8			
	( $p, nf$ )	8.7	$A/8$	1.15	1.0
	( $p, 2nf$ )	9.0			

shown in Fig. 5, although the cross section of  $^{232}\text{Pa}$  and the higher energy part of the excitation function of  $^{231}\text{Pa}$  could not be reproduced. The reason for the disagreement may be due to the neglect of the preequilibrium process in the calculation. The results of the calculation for the total asymmetric and symmetric fission cross sections are shown in Fig. 2 by dashed lines in terms of the cross section ratios. Although the agreement is poor for  $^{99}\text{Mo}$  and  $^{151}\text{Pm}$ , a general agreement is encouraging for the products with  $A_H/A_L > 1.25$  when it is considered that the model used is a very simplified one, and that the experimental data are not corrected for neutron emission. More exact theoretical calculation should include the application of the statistical model to the potential energy surface near the two kinds of saddle points with subsequent dynamical calculation to the scission point. Inclusion of the preequilibrium process in the calculation caused a decrease in the total fission cross section by 15–20% at the proton energies of 15–22 MeV, but no appreciable change in the asymmetric-to-symmetric ratio (at most 5% for the highest proton energy). The values of the parameters used in the

calculation that give the best fit to the observed data are presented in Table III. Although there were many parameters to be chosen, some of them, such as  $\hbar\omega_a$  and  $\hbar\omega_s$ , were insensitive to the fitting in this energy region. The level density parameter at the ground state deformation,  $a_n$ , was fixed to be  $A/8$  (MeV $^{-1}$ ).<sup>42</sup> The level density parameter at the saddle point configuration,  $a_f$ , need not be the same as that at ground state deformation,<sup>43–47</sup> so that the  $a_f$ 's were treated as free parameters. The  $a_f$  for symmetric fission is expected to be greater than that for asymmetric fission, since the symmetric fission becomes predominant compared to the asymmetric at higher excitation energies,<sup>10,48,49</sup> although the symmetric fission barrier height is predicted to be higher than the asymmetric.<sup>12,50,51</sup> The asymmetric fission barrier heights that gave the best fit to the data were compared with the reported values,<sup>52–54</sup> and tabulated in Table IV. The best asymmetric fission barrier heights deduced in this work are in good agreement with the experimentally observed barrier heights reported in literature. The latter may be regarded as the asymmetric fission barrier heights, since they were obtained from low energy

TABLE IV. Fission barrier heights (MeV) reported for protoactinium isotopes.

Fissioning nuclide	Vandenbosch and Seaborg (Ref. 52)	Back <i>et al.</i> (Ref. 53)	Asgher <i>et al.</i> (Ref. 54)	Present work
$^{233}\text{Pa}$	6.1 <sup>a</sup>	6.00±0.30 <sup>b</sup>		5.9 <sup>f</sup>
$^{232}\text{Pa}$	5.7 <sup>a</sup>	6.10±0.30 <sup>c</sup>	6.3 <sup>e</sup>	6.2 <sup>f</sup>
$^{231}\text{Pa}$	5.9 <sup>a</sup>	5.85±0.30 <sup>d</sup>		6.0 <sup>f</sup>

<sup>a</sup>Activation energy estimated from semiempirical consideration.

<sup>b</sup>Deduced from  $^{232}\text{Th}(^3\text{He}, df)$ .

<sup>c</sup>Deduced from  $^{231}\text{Pa}(d, pf)$ .

<sup>d</sup>Deduced from  $^{230}\text{Th}(^3\text{He}, df)$ .

<sup>e</sup>Obtained from  $^{231}\text{Pa}(n, f)$ .

<sup>f</sup>Value for asymmetric fission.

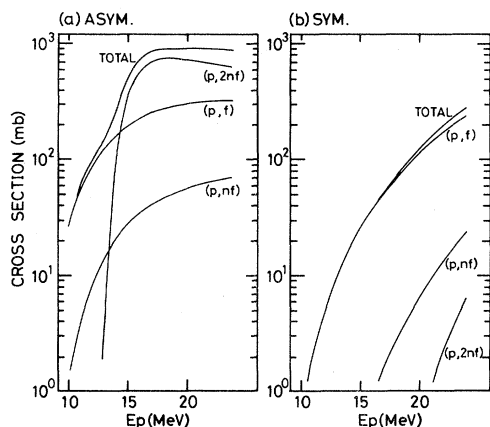


FIG. 7. Contribution of multiple chance fission in (a) asymmetric fission mode and (b) symmetric fission mode.

fission. On the other hand, the deduced symmetric fission barrier heights were found to be close to the theoretically predicted value for  $^{232}\text{Th}$ , namely, 8.8 MeV.<sup>55</sup> The calculated contribution of each multiple chance fission is shown for asymmetric fission and symmetric fission in Fig. 7(a) and Fig. 7(b), respectively. It is found that the dip in the asymmetric-to-symmetric cross section results from the contribution of the asymmetric third chance fission ( $p,2nf$ ) and that in the symmetric fission only the first chance fission ( $p,f$ ) mainly contributes in the present incident energy region.

#### IV. CONCLUSION

Excitation functions of fission products were measured for 22 fragment masses in the proton-induced fission of  $^{232}\text{Th}$  in the energy range of 8 to 22 MeV. It was found that the cross sections of symmetrically divided fission products increased monotonically with proton energy while the excitation functions of the asymmetrically divided prod-

ucts seem to exhibit some structure at 14 MeV and to level off or even decrease above 17 MeV. The cross section ratios among the symmetrically divided products were found to be essentially independent of the incident proton energy. The same results were also observed among the asymmetrically divided products. Cross section ratios of asymmetric to symmetric products (the symmetric being the average of  $^{112}\text{Pd}$  and  $^{115}\text{Cd}$ <sup>6</sup>) were plotted as a function of proton energy and found that they are strongly dependent for the products with  $A_H/A_L > 1.25$ . Detailed excitation functions of ( $p,xn$ ) reactions were also measured, especially the  $^{232}\text{Th}(p,2n)^{231}\text{Pa}$  reaction, which was measured for the first time in the present work. For the interpretation of the experimental results, the statistical evaporation-fission calculation was performed by taking symmetric and asymmetric fission barriers into consideration. In order to get the best fit to the experimental asymmetric-to-symmetric yield ratios and the excitation functions for ( $p,xn$ ) reactions, (1) the level density parameters for the symmetric ( $a_{f,s}$ ) and asymmetric saddle point ( $a_{f,a}$ ) had to be  $1.15a_n$  and  $1.02a_n$ , respectively, (2) the asymmetric fission barrier heights were 5.9, 6.2, and 6.0 MeV for ( $p,f$ ), ( $p,nf$ ), and ( $p,2nf$ ), respectively, and (3) the symmetric fission barriers, 8.8, 8.7, and 9.0 MeV for ( $p,f$ ), ( $p,nf$ ), and ( $p,2nf$ ), respectively.

The present results are consistent, although not necessarily uniquely, with a model in which two modes of mass division in fission, namely, symmetric or asymmetric, are principally determined by which saddle point configuration, reflection symmetric or asymmetric as theoretically predicted by Möller and Nilsson,<sup>12</sup> a particular fission process experiences. This interpretation is also consistent with the data on the angular distributions of fission fragments observed as a function of fragment mass.<sup>56</sup>

<sup>1</sup>O. Hahn and F. Strassman, *Naturwissenschaften* **27**, 11 (1939).

<sup>2</sup>H. W. Schmitt, *Proceedings of the 2nd IAEA Symposium on Physics and Chemistry of Fission*, Vienna, 1969, p. 67.

<sup>3</sup>F. Plasil, D. S. Burnett, H. C. Britt, and S. G. Thompson, *Phys. Rev.* **142**, 696 (1966).

<sup>4</sup>F. Plasil and H. W. Schmitt, *Phys. Rev. C* **5**, 528 (1972).

<sup>5</sup>J. P. Unik and J. R. Huizenga, *Phys. Rev.* **134**, B90 (1964).

<sup>6</sup>K. F. Flynn, L. E. Glendenin, and J. R. Huizenga, *Nucl. Phys.* **58**, 321 (1964).

<sup>7</sup>R. C. Jensen and A. W. Fairhall, *Phys. Rev.* **109**, 942

(1958).

<sup>8</sup>L. J. Colby, Jr., M. L. Shoaf, and J. W. Cobble, *Phys. Rev.* **121**, 1415 (1961).

<sup>9</sup>E. Konecny and H. W. Schmitt, *Phys. Rev.* **172**, 1213 (1968).

<sup>10</sup>I. F. Croall and J. G. Cuninghame, *Nucl. Phys.* **A125**, 402 (1969).

<sup>11</sup>H. C. Britt and S. L. Whetstone, Jr., *Phys. Rev.* **133**, B603 (1964).

<sup>12</sup>P. Möller and S. G. Nilsson, *Phys. Lett.* **31B**, 283 (1970).

<sup>13</sup>E. Konecny, H. J. Specht, and J. Weber, *IAEA Report No. IAEA SM-174/20*, 1973, Vol. II, p. 3.

- <sup>14</sup>P. Fong, *Phys. Rev.* **102**, 434 (1956); A. V. Ignatyuk, *Yad. Fiz.* **9**, 357 (1969); H. Okamoto, H. Nakahara, and T. Nishi, *J. Phys. Soc. Jpn.* **34**, 588 (1973).
- <sup>15</sup>B. D. Wilkins, E. P. Steinberg, and R. R. Chasman, *Phys. Rev. C* **14**, 1832 (1976).
- <sup>16</sup>D. C. Aumann and G. Müllen, *Nucl. Instrum. Methods* **115**, 75 (1974).
- <sup>17</sup>R. Collé, R. Kishore, and J. B. Cumming, *Phys. Rev. C* **9**, 1819 (1974).
- <sup>18</sup>C. F. Williamson, J. P. Boujot, and J. Picard, Centre d'Études Nucléaires de Saclay Report CEA-R3042, 1966 (unpublished).
- <sup>19</sup>L. C. Northcliffe and R. F. Schilling, *Nucl. Data A* **7**, 233 (1970).
- <sup>20</sup>M. V. Rananiah, R. J. Singh, S. K. Awasthi, and S. Prakash, *Intern. J. Appl. Rad. Isot.* **26**, 648 (1975).
- <sup>21</sup>F. P. Treadwell, in *Analytical Chemistry*, 9th ed., translated and revised by W. T. Hall (Wiley, New York, 1955), Vol I.
- <sup>22</sup>*Table of Isotopes*, 7th ed., edited by C. M. Lederer and V. S. Shirley (Wiley, New York, 1978).
- <sup>23</sup>J. Blachot and C. Fiche, *At. Data Nucl. Data Tables* **20**, 241 (1977).
- <sup>24</sup>J. Kleinberg, Los Alamos Scientific Laboratory Report LA-1721, 3rd ed., 1954 (unpublished).
- <sup>25</sup>C. W. Sill, *Anal. Chem.* **38**, 1458 (1966).
- <sup>26</sup>K. W. Puphal and D. R. Olsen, *Anal. Chem.* **44**, 284 (1972).
- <sup>27</sup>H. A. Tewes and R. A. James, *Phys. Rev.* **88**, 860 (1952).
- <sup>28</sup>R. W. Eaker and G. R. Choppin, *J. Inorg. Nucl. Chem.* **38**, 31 (1976).
- <sup>29</sup>B. J. Bowles, F. Brown, and J. P. Butler, *Phys. Rev.* **107**, 751 (1957).
- <sup>30</sup>R. Eaker, H. S. Plendl, A. F. Zeller, A. Clem, L. Muga, and J. M. Nicovich, *Phys. Rev. C* **20**, 1055 (1979).
- <sup>31</sup>L. E. Glendenin, J. E. Gindler, I. Ahmad, D. J. Henderson, and J. W. Meadows, *Phys. Rev. C* **22**, 152 (1980).
- <sup>32</sup>B. J. Bowles and N. Beckett, *Phys. Rev.* **147**, 852 (1966).
- <sup>33</sup>This observation was first reported by P. R. O'Connor and G. T. Seaborg, *Phys. Rev.* **74**, 1189 (1948).
- <sup>34</sup>J. A. McHugh and M. C. Michel, *Phys. Rev.* **172**, 1160 (1968).
- <sup>35</sup>A. C. Wahl, A. E. Norris, R. A. Rouse, and J. C. Williams, Proceedings of the 2nd IAEA Symposium on Physics and Chemistry of Fission, Vienna, 1969, p. 813.
- <sup>36</sup>G. H. McCormich and B. L. Cohen, *Phys. Rev.* **96**, 722 (1954).
- <sup>37</sup>H. A. Tewes, *Phys. Rev.* **98**, 25 (1955).
- <sup>38</sup>G. R. Choppin, J. R. Meriwether, and J. D. Fox, *Phys. Rev.* **131**, 2149 (1963).
- <sup>39</sup>N. Bohr and J. A. Wheeler, *Phys. Rev.* **56**, 426 (1939).
- <sup>40</sup>F. Plasil, Oak Ridge National Laboratory Report TM-6054, 1977 (unpublished).
- <sup>41</sup>D. L. Hill and J. A. Wheeler, *Phys. Rev.* **89**, 1102 (1953).
- <sup>42</sup>J. R. Huizenga and L. G. Moretto, *Annu. Rev. Nucl. Sci.* **22**, 427 (1972).
- <sup>43</sup>C. J. Bishop, I. Halpern, R. W. Shaw, Jr., and R. Vandenbosch, *Nucl. Phys.* **A198**, 161 (1972).
- <sup>44</sup>V. S. Ramamurthy, S. S. Kapoor, and S. K. Kataria, *Phys. Rev. Lett.* **25**, 386 (1970).
- <sup>45</sup>L. G. Moretto and R. Stella, *Phys. Lett.* **B32**, 558 (1970).
- <sup>46</sup>R. Vandenbosch and U. Mosel, *Phys. Rev. Lett.* **28**, 1726 (1972).
- <sup>47</sup>F. C. Williams, Jr., G. Chan, and J. R. Huizenga, *Nucl. Phys.* **A187**, 225 (1972).
- <sup>48</sup>E. F. Neuzil and A. W. Fairhall, *Phys. Rev.* **129**, 2075 (1963).
- <sup>49</sup>S. Baba, H. Umezawa, and H. Baba, *Nucl. Phys.* **A175**, 177 (1971).
- <sup>50</sup>H. C. Pauli, T. Ledergerber, and M. Brack, *Phys. Lett.* **34B**, 264 (1971).
- <sup>51</sup>M. Bolsterli, E. O. Fiset, J. R. Nix, and J. L. Norton, *Phys. Rev. C* **5**, 1050 (1972).
- <sup>52</sup>R. Vandenbosch and G. T. Seaborg, *Phys. Rev.* **110**, 507 (1958).
- <sup>53</sup>B. B. Back, H. C. Britt, O. Hansen, B. Leoux, and J. D. Garrett, *Phys. Rev. C* **10**, 1948 (1974).
- <sup>54</sup>M. Asghar, F. Caitucoli, P. Perrien, and C. Wagemans, *Nucl. Phys.* **A311**, 413 (1978).
- <sup>55</sup>P. Möller and J. R. Nix, *Nucl. Phys.* **A229**, 269 (1974).
- <sup>56</sup>H. Kudo, Y. Nagame, H. Nakahara, K. Miyano, and I. Kohno, *Phys. Rev. C* **25**, 909 (1982).